A Cyber-Secured Operation for Water-Energy Nexus

Pengfei Zhao, Chenghong Gu, *Member, IEEE,* Zhidong Cao, Da Xie, *Member, IEEE,* Fei Teng, *Member, IEEE,* Jianwei Li, Xinlei Chen, Chenye Wu, Dongmin Yu, Xu Xu, and Shuangqi Li

***Abstract*—The wide implementation of information and communication technologies (ICT) cause power system operations exposed to cyber-attacks. Meanwhile, the tendency of integrated multi energy vectors has worsened this issue with multiple energy coupled. This paper proposes a two-stage risk-averse mitigation strategy for water-energy systems (WESs), incorporating power, natural gas and water systems against false data injection attacks (FDIA) under water-energy nexus. The FDIA on individual sub-systems is modelled through hampering false data integrity to the systems. An innovative two-stage risk-averse distributionally robust optimization (RA-DRO) is proposed to mitigate uneconomic operation and provides a coordinated optimal load shedding scheme for the nexus system security. A coherent risk measure, Conditional Value-at-Risk is incorporated into the RA-DRO to model risk. A Benders decomposition method is used to solve the original NP-hard RA-DRO problem. Case studies are demonstrated on a WES under water-energy nexus and results show that the effectiveness of the method to mitigate risks from potential FDIA and renewable uncertainties. This research provides WES operators an economic system operation tool by optimally coordinating energy infrastructures and implementing reasonable load shedding to enhance cybersecurity.**

***Index Terms*—Distributionally robust optimization, false data injection attacks, integrated energy system, mitigation strategy, risk aversion, water-energy nexus.**

NOMENCLATURE

The superscript '*s*' and '*re*' representing 'scheduled' and 'regulated' respectively are omitted in section *C*. The superscript '*ini*' and '*ter*' representing initial and terminal nodes of power bus, gas and water nodes are also omitted in this section to save space.

A. Indices and sets

t, T	Index and set of time periods.
b, B	Index and set of power buses.
n, N	Index and set of gas nodes.
w, W	Index and set of water nodes.
i_e, I_e	Index and set of generators.
i_g, I_g	Index and set of gas wells.
wr, WR	Index and set of water reservoirs.
j, J	Index and set of renewable energy sources (RES).
gt, GT	Index and set of gas turbines.
wp, WP	Index and set of water pumps.
l_e, L_e	Index and set of power lines.
l_g, L_g	Index and set of gas pipelines.
l_w, L_w	Index and set of water pipelines without pumps.
l_{wp}, L_{wp}	Index and set of water pipelines with pumps.
k_e, K_e	Index and set of power loads.
k_g, K_g	Index and set of gas loads.
k_w, K_w	Index and set of water loads.

B. Parameters

AIL	Attack injection level for FDIA.
$R_{i_e}^+$, $R_{i_e}^-$, R_{gt}^+, R_{gt}^-, R_{wp}^+,R_{wp}^-	Maximum up and down reserve capacity of generators, the gas turbine and water pumps.
x_{l_e}	Resistance of power line l_e.
$f_{l_e,max}$	Maximum power flow of line l_e.
$P_{k_e,t}, G_{k_g,t}, P_{k_w}$	Demand of power, gas and water.
$\omega_j^s(t)$	Forecasted output of RES j at time t.
$G_{i_g,max}$, $G_{i_g,min}$	Maximum and minimum output of gas source i_g.
$Pr_{l_g,max}, Pr_{l_g,}$	Maximum and minimum pressure of gas pipeline l_g.
γ_{l_g}	Coefficient for Weymouth equation.
$f_{l_g,max}$,	Maximum gas flow of line l_g.
c_{gt}	Conversion coefficient for gas turbines.
η_e	Electrical efficiency for electrolyser.
$h_{w,max}^{l_{wp}}, h_{w,min}^{l_{wp}}$ $h_{w,max}^{l_w}$, $h_{w,min}^{l_w}$	Maximum and minimum limits for head pressure of water node connected with or without water pump.
$a_{l_{wp}}, b_{l_{wp}}$	Water pump characteristic coefficients.
$R_{l_{wp}}, R_{l_w}$	Head gain and loss coefficients.
π_{wp}	Water pump efficiency.
$f_{l_{wp},max}^s, f_{l_w,m}^s$	Water flow limits for water pipeline with and without pump.
$\sigma_{k_{pg}}$	Water consumption coefficient of power-to-gas.
$P_{k_e,max}^{ls} P_{k_g,max}^{ls}$, $P_{k_w,max}^{ls}$	Maximum limits of power, gas and water load shedding.
$\lambda_{i_e}^a, \lambda_{i_e}^b, \lambda_{i_e}^c$	Cost coefficients of generator i_e.
λ_{i_g}	Cost coefficient for output of gas well i_g.
λ_{wr}	Cost coefficient of water purchase.

$\lambda_{i_e}^{+}$, $\lambda_{i_e}^{-}$, λ_{GT}^{+}, λ_{GT}^{-}, λ_{wp}^{+}, λ_{wp}^{-}	Cost coefficient for up and down reserve of generators, gas turbines and water pumps.
$\lambda_{i_e}^{re}$, λ_{j}^{re}, $\lambda_{i_g}^{re}$, λ_{wr}^{re}	Regulation cost coefficient of power purchase, generators, RES, gas wells and water reservoirs.

C. Variables

$r_{i_e,t}^{+}$, $r_{i_e,t}^{-}$, $r_{gt,t}^{+}$, $r_{gt,t}^{-}$, $r_{wp,t}^{+}$, $r_{wp,t}^{-}$	Up and down reserve capacity of generators, the gas turbine and water pumps.
$P_{i_e,t}$, $P_{gt,t}$, $P_{wp,t}$	Output of generators , gas turbines and water pump power consumption.
$\theta_{l_e,t}^{ini}$, $\theta_{l_e,t}^{ter}$	Phase angle at initial and terminal buses.
$G_{i_g,t}$	Output of gas wells.
$f_{l_e,t}$, $f_{l_g,t}$	Power flow and gas flow.
$Pr_{n,t}$	Pressure of gas node *n*.
$f_{l_g,GT,t}$, $P_{gt,t}$	Injected gas flow and output of gas turbine.
$P_{n,t}^{P2G}$	Power consumed by the electrolyser.
$G_{n,t}^{hy}$	Gas output for power-to-gas process.
$P_{wr,t}$	Water purchase from reservoir.
$h_{w,t}^{l_{wp}}$, $h_{w,t}^{l_w}$,	Water pressure of pipe with and without water pump.
$\bar{h}_{w,t}^{l_w}$, $\bar{h}_{w,t}^{l_{wp}}$,	Elevation of water node connected with and without pump.
$\tilde{h}_{w,t}^{l_w}$, $\tilde{h}_{w,t}^{l_{wp}}$	Head loss and gain of water node.
$f_{l_{wp},t}$, $f_{l_w,t}$	Water flow of pipe with and without water pump.
$\Delta P_{k_e,t}$, $\Delta P_{k_g,t}$, $\Delta P_{k_w,t}$	Load deviation due to FDIA.
$P_{k_e,t}^{ls}$, $P_{k_g,t}^{ls}$, $P_{k_w}^{ls}$	Load shedding of power, gas and water.
$\xi_{j,t}$	Generation of renewable energy sources.

I. INTRODUCTION

MODERN energy management systems (EMS) with the increasing dependence on emerging information and communication technologies (ICTs), have massively facilitated the high efficiency, reliability and security of the EMS [1]. Meanwhile, the increasingly aggressive cyber-attacks are also growing in numbers. As a typical arbitrary cyber-attack, false data injection attack (FDIA) can be manipulated by adversaries to integrate falsified data into real-time meter measurement and thus to affect and mislead the system operators with erroneous decisions on operation and control [2, 3].

Present research work of investigating FDIA on EMS can be categorized in terms of the perspective of attackers or system defenders. As for attack modelling from adversaries, a class of unobservable FDIA are designed assuming the attacker has the knowledge of system historical data [4]. A generalized framework for investigating the vulnerability of power system nonlinear state estimator to FDIA is analysed in [5]. Meanwhile, a robust detector model is proposed to check the measurement statistical consistency with the ensured detectability. From the perspective of system defenders, detection modelling and corresponding algorithms have been investigated widely. State estimation is of great significance in EMS, which provides reliable state estimates for system operators on economic dispatch and reliability analysis [6]. State estimation is implemented based on redundant measurements to filter out corrupted data. Nevertheless, some judiciously designed FDIA can be masked and hidden and eventually bypass the state estimation.

Therefore, mitigation strategy for EMS against FDIA is considered as the final barrier for defending power systems since conventional state estimation is still employed which fails to detect stealthy designed FDIA in real practice. The mitigation strategy for intra-interval operational security against FDIA is proposed in [7]. A dynamic analytical framework is designed for analysing the impacts considering system variability in the short dispatch interval. Paper [8] proposes the mitigation strategy for a unit commitment by using a tri-level optimization model and the original problem is transformed into a bi-level mixed-integer programming. The previous work of the authors proposes a risk and mitigation strategy for integrated electricity and gas systems under FDIA in a moment-based hierarchical two-stage framework [9]. In comparison, the improvements of this paper over [9] are three aspects: i) water-energy nexus has gained extensive research attention. There is widely investigation of FDIA on power systems. However, WESs also require a cyber-secured operation scheme against FDIA. Since WESs are more vulnerable than power systems or IESs with higher interdependencies; ii) the proposed WES is linked closer via power-to-gas (P2Gs), gas turbines and water pumps than with only one gas turbine. The complex couplings and interconnections among power, gas and water systems desire a cyber-secured operation scheme; iii) a risk-averse DRO is adopted in this paper considering the risk of uneconomic operation cost caused by FDIA and renewable uncertainties. However, paper [9] lacks risk analysis. Compared with the existing risk mitigation strategy against FDIA, the advancement of this paper is summarized in TABLE I.

The interdependencies between coupled energy systems have been largely promoted due to the rapid demand increase of multiple energy and the development of energy conversion technologies. Through fully exploiting the interdependency of integrated energy systems (IES), existing literature regarding IES operation mainly focuses on several aspects: i) economic-based operation for minimizing operation cost or maximizing economic gain under normal conditions, ii) reliability-based operation considering risks from reliability issues and iii) resilience-based operation strategies against natural disasters. Paper [10] proposes an economic system operation for IES considering the relief of power and gas flow congestions. The distributed optimization outperforms than centralized optimization method with parallel data processing. A security-constrained unit commitment is designed in [11] for enhancing the operational reliability of IES considering possible *N - k* contingencies. A two-stage RO is applied and the problem is solved by a second-order cone-based Column & Constraint Generation (CCG) approach.

TABLE I
COMPARING THE PROPOSED MODEL WITH DIFFERENT STUDIES

Reference No.	Test system			**Water-energy nexus**	Risk mitigation approach	Optimization framework	FDIA			Renewable uncertainty
	Power	Gas	Water				Power	Gas	Water	
[4]	✓	×	×	×	Single-stage	Deterministic	✓	×	×	×
[12]	✓	×	×	×	Single-stage	Deterministic	✓	×	×	×
[37]	✓	×	×	×	Single-stage	Deterministic	✓	×	×	×
[13]	✓	×	×	×	Single-stage	Robust	✓	×	×	×
[14]	✓	✓	×	×	Two-stage	DRO	✓	✓	×	✓
Proposed	✓	✓	✓	✓	Two-stage	Risk-averse DRO	✓	✓	✓	✓

In recent studies, the novel distributionally robust optimization (DRO) is widely deployed to overcome the disadvantages of RO and SO. DRO employs partial distribution information instead of requiring the specific full knowledge of distributions [12, 13]. Meanwhile, it is a data-driven approach, which yields less-conservative solutions than RO. A combined optimization for integrated electricity and heat systems is proposed in [14] considering renewable and ambient temperature uncertainties, which are characterized by DRO. Paper [15] investigates the operation schemes for energy hub systems (EHSs) considering renewable uncertainty and multimodality information.

The uncertainties bring risks into economic operation. Intuitively, risks in the proposed WES operation model can lead to abnormal high operation cost. Risk-averse optimization considers a coherent trade-off between system economic performance and risk, which has been applied with SO on energy system operation [16, 17]. Paper [16] develops a risk-averse stochastic programming model for unit commitment considering renewable energy uncertainty. A conditional value-at-risk (CVaR) is incorporated to assess the risk from renewable energy uncertainty. In [17], a day-ahead operational planning model for a regional energy service provider with electricity price uncertainty is proposed. The CVaR criterion is employed to hedge against the uncertainty. This paper utilizes a risk-averse DRO model, which outperforms the existing risk-averse SO models with more practical distributional information availability.

Under the era of water-energy nexus, water systems have been given higher attention in the recent research works. Traditionally, water and power systems are modelled and operated separately. However, the two systems are actually mutually interdependent [18]. Around 80% of the power consumed in water systems is used for pumping and distributing water [19]. In power systems, surplus water resources significantly contribute to the generation and conversion in power systems. The joint optimization of power and water systems have been investigated in existing work, targeting at reducing operation cost and emissions. An optimal water-power usage operation scheme is in [20] considering the couplings in an integrated power and water system (IPWS). An alternating direction method of multipliers-based optimization is used. Paper [21] utilizes the water as an effective resource to manage renewable generators combined with demand-side management. Very recent work proposes a two-stage robust optimization (RO) model for multi energy systems [22]. Wind uncertainty is handled and the proposed model is solved by a CCG method.

In this paper, the proposed water-energy system (WES) incorporates power, gas and water systems. It realizes the comprehensive coordination between energy infrastructures of the three independent systems. The increasing penetration of conversion technologies strengthen the coupling and interactions between electricity, gas and water systems. The interdependency is enhanced, leading to both beneficial and adverse impacts for WES. As for the beneficial impacts, the relatively lower price of gas sources can provide more economic operation solutions for WES; the surplus generation in the original independent energy system can supply loads in other sub-energy systems based on upcoming energy conversions. However, the strong interdependency of WES is detrimental to system security, i.e., reliability issues, natural disasters and cyber-attacks. The failure on power, gas or water systems will inevitably propagate to other sub-systems. Accordingly, the uneconomic operation is caused not only because of the individual complexities in each sub-system, but also due to the tight interdependencies. The higher the interdependency in a WES, the more vulnerable the WES is.

This paper proposes a risk-averse mitigation strategy to alleviate the uneconomic operation of WES against potential FDIA considering renewable uncertainty. FDIA is assumed to target at load meter readings of power, gas and water systems. The two-stage framework consists of i) day-ahead operation scheme prior to the FDIA and forecasting of renewable uncertainty and ii) the implementation of real-time recourse actions based on the FDIA and realization of renewable uncertainty. Load shedding and scheduling operation are considered as the recourse actions to mitigate the impact from FDIA. The ambiguity set for capturing the FDIA and renewable uncertainty is constructed based on Kullback-Leibler (KL) divergence. The coherent risk measure, i.e., CVaR is used to balance the trade-off between risk and computational performance. The proposed two-stage risk-averse distributionally robust FDIA mitigation strategy for WES is denoted as TSRA-FMS for simplicity. Bender's decomposition approach is adopted to solve the TSRA-FMS problem.

The major contributions of this paper are as follows:

1) This paper develops a mitigation strategy against FDIA for WES. The water-energy nexus achieves optimal energy coordination under normal conditions but is more vulnerable to cyber-attacks. The interdependencies between power, gas and water systems are analysed under different FDIA scenarios.

2) It utilizes a two-stage optimization framework

incorporating both day-ahead system operation under normal conditions and real-time mitigation scheme against potential FDIA. To defend and mitigate the FDIA, capacity reserve from generations are scheduled in the first stage and load shedding is implemented in the second stage.

3) The model incorporates CVaR into DRO. This risk-averse mitigation method has the benefits of: i) it inherits the advantages of RO and SO based on limited uncertainty distribution information with weakened robustness, ii) compared with moment-based ambiguity set, the ambiguity set constructed by KL divergence can flexibly shape the candidate distributions of both FDIA and renewable uncertainty and thus it yields less-conservative solutions and iii) the trade-off between the optimization performance and risk is modelled based on the incorporation of CVaR.

The remaining paper is organized as follows: section II models three types of FDIA in power, gas and water systems. The problem formulation of TSRA-FMS is given in section III. In section IV, the methodology of KL divergence-based TSRA-FMS considering CVaR as the risk measure is proposed. The case studies are given in section V. Section VI concludes the paper.

II. Attack Modelling

This paper considers three types of FDIA and the attack modelling is in this section. State estimation is used to provide accurate snapshot of power systems and detect FDIA based on available measurements. Nevertheless, a stealthy designed FDIA can be undetectable and bypass the state estimation. The FDIA considered in this paper is designed on corrupting load measurement. Equation (1) and (2) show the original expression of bus power injection and line flow. The incidence matrices of bus-generator and bus-load are represented by KP and KD, respectively. The shift factor matrix can be obtained from the linearized DC flow equation, which is used to approximate the change of active power flow. The incremental matrices of BP and PL are given in (3) and (4) due to FDIA.

$$BP = KP \cdot G - KD \cdot D \tag{1}$$

$$PL = SF \cdot BP \tag{2}$$

$$\Delta BP = KP \cdot \Delta G - KD \cdot \Delta D \tag{3}$$

$$\Delta PL = SF \cdot \Delta BP \tag{4}$$

The following conditions should be satisfied for a successful FDIA:

Condition 1:$\Delta G = 0$. The attack on the measurement of output of generation is ignored since this type of attack can be easily detected and corrected.

Condition 2: Zero injection buses, i.e., buses without generators or loads connected, are not attackable.

Condition 3: Load measurements are attackable.

Condition 4: The load measurement eventually impacts on branch flow measurement.

The resulting formulation in (5) is obtained based on the above conditions:

$$\Delta PL = -SF \cdot KD \cdot \Delta D \tag{5}$$

As proposed in [23], the FDIA targeting on the load measurements increases and decreases some loads simultaneously. And the total load is remained unchanged. The attack deviation is limited with the attack injection level *AIL* in (7).

$$\sum \Delta D = 0 \tag{6}$$

$$-AIL\ D \le \Delta D \le AIL\ D \tag{7}$$

Constraint (8) and (9) limit the original and attacked power flow before and after the FDIA. However, in practice, the line capacity is always sufficiently large in case of overloading issues.

$$\underline{PL} \le PL \le \overline{PL} \tag{8}$$

$$\underline{PL} + SF \cdot KD \cdot \Delta D \le PL \le \overline{PL} + SF \cdot KD \cdot \Delta D \tag{9}$$

In the real implementation, constraints (10) and (11) are used as the explicit expressions of (6) and (7).

$$\sum \Delta P_{k_e,t} = 0 \tag{10}$$

$$-AIL_{k_e} P_{k_e,t} \le \Delta P_{k_e,t} \le AIL_{k_e} P_{k_e,t} \tag{11}$$

To investigate the system interdependencies under the exposure of FDIA, the FDIA on load measurement of gas and water systems are additionally considered, which are given in (12) and (13).

$$-AIL_{k_a} P_{k_a,t} \le \Delta P_{k_a,t} \le AIL_{k_a} P_{k_a,t} \tag{12}$$

$$-AIL_{k_w} P_{k_w,t} \le \Delta P_{k_w,t} \le AIL_{k_w} P_{k_w,t} \tag{13}$$

III. Cyber-Secured Mitigation Scheme

The proposed two-stage cyber-secured mitigation scheme for the uneconomic operation of WES includes: i) day-ahead operation scheme prior to the FDIA and renewable uncertainty and ii) real-time corrective redispatch scheme and security measures under the potential FDIA and the realization of renewable uncertainty. This section proposes the objective function of the mitigation scheme and the associated constraints.

A. WES Structure

The proposed WES structure is shown in Fig. 1, including a modified IEEE 30-bus power system, a 20-node gas system and a 10-node water system. The power system contains 5 power generators and 3 RES generators. Two P2G facilities interconnect RES generators and gas nodes, which converts the excessive power energy to hydrogen gas. A gas turbine transfers gas from node 8 to bus 13. In the water system, there are 2 water reservoirs and 3 water pumps. Water pumps connected with nodes 1, 2 and 6 consume power form buses 29 and 30. The water electrolysers of P2Gs consume water, which are supplied from node 5. It is to be noted that the gas and water nodes are similar to the electrical buses in power systems. Nodes are the points that connect two or more gas pipelines, where a certain volume of gas is delivered or injected. A typical gas node can be connected with gas pipelines, natural gas sources, gas wells, gas storage systems, gas compressors and gas loads. In water networks, the water pipelines and nodes are similar to the power lines and buses in power networks, which are used to describe pipe connections and endings. Water nodes in a water network can represent water supplies, storage, pumps and loads.

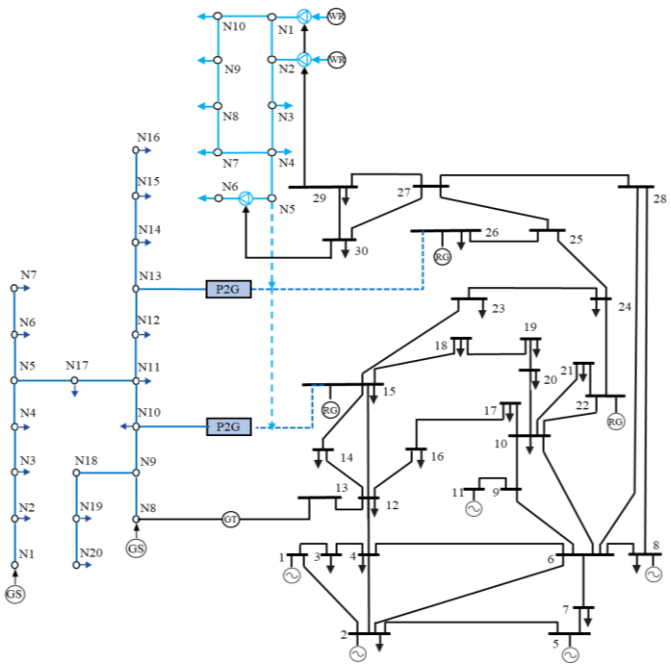

Fig. 1. The structure of WES.

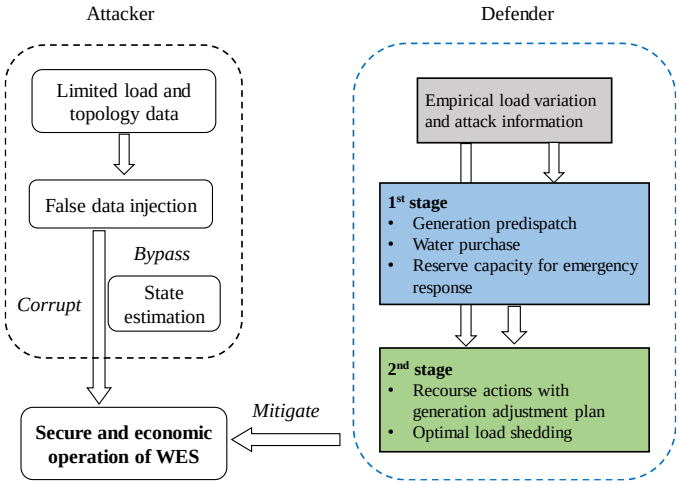

Fig. 2. The proposed cyber-secured mitigation scheme.

B. Objective Function

The overall objective is to mitigate the uneconomic operation, which is separated into a hierarchical day-ahead and real-time optimization under normal conditions and FDIA, respectively. The structure of the proposed cyber-secured mitigation scheme is given in Fig. 2. The objective function of day-ahead operation is given in (14), including the i) day-ahead generation cost of electricity generators, gas wells, ii) reserve cost of generators, gas turbines and water pumps and iii) water purchase cost from reservoirs. It is to be noted that the reserve capacity is prepared for counteracting impacts from FDIA and renewable uncertainty in the second stage.

$$\Gamma_1 = \min \sum_{i_e\in I_e, i_g\in I_g, t\in T} \lambda^a_{i_e} {P^s_{i_e,t}}^2 + \lambda^b_{i_e} P^s_{i_e,t} + \lambda^c_{i_e} + \lambda_{i_g} P^s_{i_g,t} + \lambda_{wr} P^s_{wr,t} + \lambda^+_{\{\cdot\}} r^+_{\{\cdot\},t} + \lambda^-_{\{\cdot\}} r^-_{\{\cdot\},t}, \{\cdot\} = i_e, gt, wp \quad (14)$$

The second-stage sub-objective (15) is implemented under the presence of FDIA and renewable uncertainty, which involves i) the adjustive decisions on redispatching generators, gas wells, RESs and water purchase and ii) minimum joint load shedding.

$$\Gamma_2 = \min \sum_{i_e\in I_e, i_g\in I_g, t\in T, k_e\in K_e, k_g\in K_g} +\lambda^{re}_j \left|\omega^s_{j,t} - \xi_{j,t}\right| + \lambda^{re}_{i_e}\left|P^s_{i_e,t} - P^{re}_{i_e,t}\right| + \lambda^{re}_{i_g}\left|P^s_{i_g,t} - P^{re}_{i_g,t}\right| + \lambda^{re}_{wr}\left|P^s_{wr,t} - P^{re}_{wr,t}\right| + \lambda^{ls}_{k_e} P^{ls}_{k_e,t} + \lambda^{ls}_{k_g} P^{ls}_{k_g,t} + \lambda^{ls}_{k_w} P^{ls}_{k_w,t} \quad (15)$$

C. Day-ahead operation

The day-ahead operation determines the power generation schedule of generators and the reserve dispatch of generators, gas turbines and water pumps. The day-ahead operation scheme (16)-(39) is based on the renewable forecast without considering the risks of FDIA. The reserve capacity of generators, gas turbines and water pumps are limited in (16) and (17). Constraints (18) and (19) provide the limits of output of generators, gas turbines and power consumption of water pumps. The DC power flow after the linearization is shown in (20) and (21). The power balance constraint is given in (22). Equation (23) regulates the output of gas wells.

In the gas system, gas pressure is constrained in (24). In constraint (25), it shows that the pressure at initial nodes are always larger than the terminal nodes because the gas system considered in this paper is of radial topology. Weymouth gas flow equations are given in (26) and (27). Equation (28) is the constraint of the output of gas turbines. P2G enables to utilize the surplus renewable power generation and convert it to gas. Equation (29) shows the gas output via P2G [24]. The gas nodal balancing equation is given in (30).

Equations (31)-(39) are constraints of water system. The output of water reservoir is limited in (31). The water pressure limit is given in (32) for pipes with and without water pumps. Constraints (32)-(44) describes the hydraulic characteristics of water pipes with and without water pumps including head gain and loss. In (35), the pressure head gain of water pump is shown. The hydraulic characteristic of pipes without water pumps is given in (36) based on Darcy-Weisbach equation [25]. Equation (37) presents the power consumption of water pump. The water flow magnitude is limited in (38). And the mass balance constraint of water system is presented in (39).

$$0 \le r^+_{\{\cdot\},t} \le R^+_{\{\cdot\}},\ \{\cdot\} = i_e, gt, wp \quad (16)$$

$$0 \le r^-_{\{\cdot\},t} \le R^-_{\{\cdot\}},\ \{\cdot\} = i_e, gt, wp \quad (17)$$

$$P^s_{\{\cdot\},t} + r^+_{\{\cdot\},t} \le P_{\{\cdot\},max},\ \{\cdot\} = i_e, gt, wp \quad (18)$$

$$P_{\{\cdot\},min} \le P^s_{\{\cdot\},t} - r^-_{\{\cdot\},t},\ \{\cdot\} = i_e, gt, wp \quad (19)$$

$$x_l f^s_{l_e,t} = \left(\theta^{s,ini}_{l_e,t} - \theta^{s,ter}_{l_e,t}\right) \quad (20)$$

$$-f^s_{l_e,max} \le f^s_{l_e,t} \le f^s_{l_e,max} \quad (21)$$

$$\sum_{i_e\in I_e} P^s_{i_e,t} + \sum_{j\in J} \omega^s_{j,t} + \sum_{l_e\in L_e} f^{s,ini}_{l_e,t} - \sum_{l_e\in L_e} f^{s,ter}_{l_e,t} + P^s_{gt,t} = \sum_{k_e\in K_e} P_{k_e,t} + \sum_{l_e\in L_e} f^{s,inj}_{l_e,t} + \sum_{n\in N} P^{s,P2G}_{n,t} + \sum_{wp\in WP} P^s_{wp,t} \quad (22)$$

$$G_{i_g,min} \le G^s_{i_g,t} \le G_{i_g,max} \quad (23)$$

$$Pr^2_{n,min} \le Pr^{s^2}_{n,t} \le Pr^2_{n,max} \quad (24)$$

$$Pr^{s,ini}_{n,t} \ge Pr^{s,ter}_{n,t} \quad (25)$$

$$f^{s}_{l_g,t}{}^2 = \gamma_{l_g}\left(Pr^{s,ini^2}_{n,t} - Pr^{s,ter^2}_{n,t}\right) \quad (26)$$

$$0 \le f^s_{l_g,t} \le f^s_{l_g,max} \quad (27)$$

$$P^s_{gt,t} = c_{GT} f^s_{l_g,gt,t} \quad (28)$$

$$G^{s,hy}_{n,t} = \eta_e \frac{P^{s,P2G}_{n,t}}{\Omega_{hy}} \quad (29)$$

$$\sum_{i_g\in I_g} G^s_{i_g,t} + \sum_{n\in N} G^{s,hy}_{n,t} + \sum_{l_g\in L_g} f^{s,ini}_{l_g,t} - \sum_{l_g\in L_g} f^{s,ter}_{l_g,t} = \sum_{k_g\in K_g} G_{k_g,t} + \sum_{l_g\in L_g} f^s_{l_g,gt,t} \quad (30)$$

$$0 \le P^s_{wr,t} \le P_{wr,max} \quad (31)$$

$$h^{\{\cdot\}}_{w,min} \le h^{s,\{\cdot\}}_{w,t} \le h^{\{\cdot\}}_{w,max}, \{\cdot\} = l_w, l_{wp} \quad (32)$$

$$\tilde{h}^s_{\{\cdot\},t} = \left(h^{s,\{\cdot\},ini}_{w,t} + \bar{h}^{s,\{\cdot\},ini}_{w,t}\right) - \left(h^{s,\{\cdot\},ter}_{w,t} + \bar{h}^{s,\{\cdot\},ter}_{w,t}\right), \{\cdot\} = l_w, l_{wp} \quad (33)$$

$$\tilde{h}^s_{l_{wp},t} \ge 0 \quad (34)$$

$$\tilde{h}^s_{l_{wp},t} + a_{l_{wp}} f^s_{l_{wp},t} + b_{l_{wp}} = R_{l_{wp}} f^{s}_{l_{wp},t}{}^2 \quad (35)$$

$$\tilde{h}^s_{l_w,t} = R_{l_w} f^{s}_{l_{wp},t}{}^2 \quad (36)$$

$$P^s_{wp,t} = \left(a_{l_{wp}} f^{s}_{l_{wp},t}{}^2 + b_{l_{wp}} f^s_{l_{wp},t}\right)/\pi_{wp} \quad (37)$$

$$0 \le f^s_{\{\cdot\},t} \le f^s_{\{\cdot\},max}, \{\cdot\} = l_w, l_{wp} \quad (38)$$

$$\sum_{wr\in WR} P^s_{wr,t} + \sum_{\{\cdot\}\in L_w, L_{wp}} f^{s,ini}_{\{\cdot\},t} - \sum_{\{\cdot\}\in L_w, L_{wp}} f^{s,ter}_{\{\cdot\},t} = \sum_{k_{pg}\in K_{pg}} \sigma_{k_{pg}} P^{s,P2G}_{n,t} + \sum_{k_w\in K_w} P_{k_w,t} \quad (39)$$

D. Real-time Cyber-Secured Mitigation

The cyber-secured mitigation is implemented in the second stage to mitigate the uneconomic operation based on the realization of FDIA and renewable uncertainty. Equation (40) is the regulated output of generators, gas turbines and the regulated power consumption of water pumps. Equations (41)-(44) model the stealthy designed FDIA on power, gas and water systems. The load shedding is given in (45).

$$P^s_{\{\cdot\},t} - r^-_{\{\cdot\},t} \le P^{re}_{\{\cdot\},t} \le P^s_{\{\cdot\},t} + r^+_{\{\cdot\},t},\ \{\cdot\} = i_e, gt, wp \quad (40)$$

$$\sum \Delta P_{k_e,t} = 0 \quad (41)$$

$$-\beta_{k_e} P_{k_e,t} \le \Delta P_{k_e,t} \le \beta_{k_e} P_{k_e,t} \quad (42)$$

$$-\beta_{k_g} P_{k_g,t} \le \Delta P_{k_g,t} \le \beta_{k_g} P_{k_g,t} \quad (43)$$

$$-\beta_{k_w} P_{k_w,t} \le \Delta P_{k_w,t} \le \beta_{k_w} P_{k_w,t} \quad (44)$$

$$0 \le P^{ls}_{\{\cdot\},t} \le P^{ls}_{\{\cdot\},max},\ \{\cdot\} = k_e, k_g, k_w \quad (45)$$

The rest of the second-stage constraints are not listed due to space limitation. The constraints of the second stage are the same as the first-stage constraints when the superscript '*s*' is replaced by '*re*', which denotes the regulated decision variables.

IV. Methodology

The proposed TSRA-FMS is a two-stage DRO framework with minmax formulation in the second stage problem. The linear TSRA-MS is firstly represented by compact form for notation brevity. Then the KL divergence-based ambiguity set of DRO is constructed to capture the FDIA and renewable uncertainty. In section *C*, the expression of CVaR is given and incorporated in the original formulation of TSRA-FMS. Finally, the mathematical reformulation is made and the solution algorithm is proposed.

A. Formulation in Brevity

Matrices and vectors are used for notation brevity of the TSRA-FMS problem. The original objective function of TSRA-FMS is given in (46) without considering the risk measure.

$$\min_{x\in X} c'x + \sup_{p\in D_\xi} E_p[Q(x,\xi)] \quad (46)$$

The risk-averse DRO incorporates the risk measure in the second-stage problem, which is given in (47). The first term $c'x$ is the first-stage objective. The second term $(1-\alpha)E_p[Q(x,\xi)]$ represents the weighted expected second-stage objective and the last term $\alpha R\big(Q(x,\xi)\big)$ is the weighted risk measure. The weighting coefficient α ranges between 0 and 1. Equation (50) degrades to risk-neutral DRO model when α=0.

$$\min_{x\in X} c'x + \sup_{p\in D_\xi}\{(1-\alpha)E_p[Q(x,\xi)] + \alpha R\big(Q(x,\xi)\big)\} \quad (47)$$

$$\text{s.t. } Ax \le b, \quad (48)$$

$$Q(x,\xi) = \min_y f'y \quad (49)$$

$$\text{s.t. } Ex + Fy + G\xi \le h, \quad (50)$$

The first-stage constraints are represented by (48). Equations (49) and (50) represent the second-stage objective function and constraints, respectively, where the coefficient of (49) is denoted by *f*.

B. Constructing the Ambiguity Set

Based on the distance between probability distributions, the discrepancy-based ambiguity set can be modelled, where η is the divergence tolerance. In (51) and (52), p and p_{ref} are the true and reference probability distribution, respectively. Equations (51) and (52) are the implicit and explicit descriptions of distribution distance.

$$Dis = \{p \in D_{\xi,} | D_{\xi,}(p\|p_{ref}) \le \eta\} \quad (51)$$

$$D_{\xi,}(p\|p_{ref}) = \int f(\xi)\, log\frac{p(\xi)}{p_{ref}(\xi)} d\xi \quad (52)$$

Equation (54) shows the KL-divergence function of variable *a*.

$$\varphi_{KL}(a) := a\log a - a + 1 \quad (53)$$

C. Risk-Averse DRO

CVaR refers to a risk assessment which quantifies the tail risk of investment [26]. CVaR is developed to mitigate the shortcomings of value at risk. CVaR is initially applied in finance industries, which is then extended to portfolio problems in other fields, such as power systems [27].

The probability of $Q(x,\xi)$ is limited by the threshold ζ. The coherent risk measure CVaR is convex and monotonic. The probability of $Q(x,\xi)$ not larger than the threshold ζ is shown as:

$$\Psi(x,\zeta) := \int_{Q(x,\xi)\le\zeta} p(\xi)d\xi \tag{54}$$

Where Ψ is the cumulative distribution function of $Q(x,\xi)$, which is a fundamental element of VaR and CVaR. Moreover, is continuous and nondecreasing with respect to ζ. The definition of β-VaR and β-CVaR are shown as (55) and (56).

$$VaR_\beta(Q(x,\xi)) = \min\{\zeta \in \mathbb{R}:\ \Psi(x,\zeta) \ge \beta\} \tag{55}$$

$$CVaR_\beta(Q(x,\xi)) := \frac{1}{1-\beta}\int_{Q(x,\xi)\ge\zeta_\beta(x,\xi)} Q(x,\xi)p(\xi)d\xi \tag{56}$$

Since $Q(x,\xi)$ is continuously differentiable and convex, the below formula can be derived [26, 28].

$$CVaR_\beta(Q(x,\xi)) := \min_{\zeta\in\mathbb{R}}\left\{\zeta + \frac{1}{1-\beta}E_p[Q(x,\xi)-\zeta]^+\right\} \tag{57}$$

Where function $[Q(x,\xi)-\zeta]^+$ is used to determine the larger value between $Q(x,\xi)-\zeta$ and 0.

$$[Q(x,\xi)-\zeta]^+ = \begin{cases} Q(x,\xi)-\zeta & (Q(x,\xi)-\zeta > 0) \\ 0 & (Q(x,\xi)-\zeta \le 0) \end{cases} \tag{58}$$

The original objective function of TSRA-FMS is reformulated as (59) with weighted CVaR. When substituting CVaR in (59) with (58), (59) can be derived.

$$\min_{x\in X} c'x + \sup_{p\in D_\xi, \xi=\Delta P_k, \xi_j}\{(1-\alpha)E_p[Q(x,\xi)] + \alpha CVaR_\beta(Q(x,\xi))\} \tag{59}$$

$$\min_{x\in X}\left\{c'x + \sup_{p\in D_\xi,\xi=\Delta P_k,\xi_j}\min_{\zeta\in\mathbb{R}}\{\alpha\zeta + E_p[G(x,\xi)]\}\right\} \tag{60}$$

$$G(x,\xi) := (1-\alpha)[Q(x,\xi)] + \frac{\alpha}{1-\beta}\tilde{a}$$

$$\text{s.t.} Q(x,\xi) - \tilde{a} - \zeta \le 0,\ \tilde{a} \ge 0$$

When the strong duality holds, (60) can be reformulated to (61) and then further equivalent to (62) [29].

$$\min_{x\in X}\left\{c'x + \min_{\zeta\in\mathbb{R}}\sup_{p\in D_\xi,\xi=\Delta P_k,\xi_j}\{\alpha\zeta + E_p[G(x,\xi)]\}\right\} \tag{61}$$

$$\min_{x\in X}\left\{c'x + \alpha\zeta + \max_{p\in D_\xi,\xi=\Delta P_k,\xi_j}\left\{\sum_{i=1}^m p_i G_i(x,\xi)\right\}\right\} \tag{62}$$

Larange function (63) can be used to handle the inner maximization problem with its dual formulation (64).

$$\mathcal{L}(p,\tau,\mu) = \sum_{i=1}^m p_i G_i(x,\xi) + \tau\left(1-\sum_{i=1}^m p_i\right) + \mu\left(\eta - \sum_{i=1}^m p_{ref,i}\,\varphi_{KL}\left(\frac{p_i}{p_{ref,i}}\right)\right) \tag{63}$$

$$\max\ \mathcal{L}(p,\tau,\mu) = \tau + \eta\mu + \mu\sum_{i=1}^m p_{ref,i}\left[\exp\left(\frac{G_i(x,\xi)-\tau}{\mu}\right)-1\right] \tag{64}$$

Based on the Slater's condition [30], the (65) and (66) can be made when η is larger than 0:

$$\max_{p\in D_\xi,\xi=\Delta P_k,\xi_j}\left\{\sum_{i=1}^m p_i G_i(x,\xi)\right\} = \min_{\tau,\mu\ge 0}\max\ \mathcal{L}(p,\tau,\mu) \tag{65}$$

$$= \min_{\tau,\mu\ge0}\left\{\tau + \eta\mu + \mu\sum_{i=1}^m p_{ref,i}\left[\exp\left(\frac{G_i(x,\xi)-\tau}{\mu}\right)-1\right]\right\} \tag{66}$$

The derivation in (67) can be obtained when substituting the inner maximization problem in (62) with (66).

$$\min_{\zeta,\tau,\mu\ge0}\left\{c'x + \alpha\zeta + \tau + \eta\mu + \mu\sum_{i=1}^m p_{ref,i}\left[\exp\left(\frac{G_i(x,\xi)-\tau}{\mu}\right)-1\right]\right\} \tag{67}$$

$$\text{s.t. } x\in X,\ Q(x,\xi) - \tilde{a} - \zeta \le 0,\ \tilde{a}\ge 0,$$

$$G(x,\xi) := (1-\alpha)[Q(x,\xi)] + \frac{\alpha}{1-\beta}\tilde{a}$$

Nevertheless, equation (67) is a nonlinear problem which requires to be linearized before the decomposition algorithm. For a given $x = x^k$, when $Q(x^k,\xi) < \infty$, $Q(x^k,\xi)$ is subdifferentiable [31] and (68) can be obtained, where $Dual(x^k) = arg\max\{\pi'(h-Ex^k): F'\pi \le f\}$ is the set of optimal solutions of dual problem in (49). $\pi^{k,i} \in Dual(x^k)$ is the optimal solution for the ith scenario and kth iteration.

$$\partial Q(x^k,\xi) = -E'Dual(x^k) \tag{68}$$

Let $s^k := \frac{G_i(x^k,\xi)-\tau^k}{\mu^k}$ and $F_i^k := \mu^k[\exp(s^k)-1]$, the subgradient of F_i^k is given as:

$$\partial F_i^k = \left[(1-\alpha)\exp(s^k)E'\pi^{k,i}, (1-s^k)\exp(s^k)-1, -\exp(s^k), \frac{\alpha}{1-\beta}\exp(s^k)\right] \tag{69}$$

Equation (70) can be obtained based on the subgradient inequality of convex function. And equation (71) is the optimality cut.

$$F_i(x,\mu,\tau,\tilde{a}_i) \ge F_i(x^k,\mu^k,\tau^k,\tilde{a}_i^k) + \partial F_i^k\cdot(x-x^k,\mu-\mu^k,\tau-\tau^k,\tilde{a}_i-\tilde{a}_i^k) \tag{70}$$

$$F_i(x,\mu,\tau,\tilde{a}_i) \ge \left[G_i(x^k,\xi) + (1-\alpha)(\pi^{k,i})'Ex^k - \frac{\alpha\tilde{a}_i^k}{1-\beta}\right] + \partial F_i^k(x,\mu,\tau,\tilde{a}_i) \tag{71}$$

Finally, to solve the overall two-stage risk-averse DRO problem, a Bender's decomposition method should be applied.

V. CASE STUDY

In this section, the numerical experiments are validated on a modified IEEE 30-bus power system, connected with a 20-node gas system and a 10-node water system. The WES is given in Fig. 1. The RESs are connected at buses 15, 22 and 26 with 60MW for each output. Two P2G facilities and a gas turbine are used for power-gas connection. The water consumption of P2Gs is supplied by the water system at node 5. The water system has three water pumps, which consume power from the power system. TABLEs II presents the parameters of water reservoirs. Fig. 3 presents the maximum and minimum limits of the gas pressure. The load profile of power, gas and water systems are shown in Figs. 4-5. For notation simplicity, the FDIA at power, gas and water systems are denoted as P-FDIA, G-FDIA and W-FDIA, respectively.

The case illustration is given in TABLE III. Case 1 is a deterministic operation model of WES without considering FDIA or renewable uncertainty. Case 2 utilizes RO to capture FDIA. Compared with case 2, case 3 further incorporates renewable uncertainty. Cases 4-7 are used to analyse the impact under different FDIA scenarios. As the benchmark case, case 7 considers all the potential types of FDIA (P-FDIA, G-FDIA and W-FDIA) with 5% of *AIL*. In comparison, the *AIL* of cases 8-10 gradually increases.

A. Studies on Economic Performance

The economic performance for all cases are first analysed and the result is given in TABLE IV. Case 1 has the lowest operation cost, i.e., \$843986, when no FDIA is conducted. In contrast, the operation cost of case 10 is the highest (\$2521441) when all three types of FDIA are at 20% of *AIL*. Compared with cases 6 and 7, cases 2 and 3 utilize single-stage RO. The results of cases 2 and 3 are higher than cases 6 and 7, which implies the over-conservatism of RO when considering the worst-case FDIA condition. Case 4 only considers the potential impact from P-FDIA, which yields the second-lowest solution, i.e., \$855096. When addition G-FDIA is modelled in case 5, the operation cost is \$26866 higher than that of case 4. Similarly, W-FDIA and renewable uncertainty are additionally considered in cases 6 and 7. The *AIL* is increasing consecutively in cases 7, 8, 9 and 10 from 5% to 20%. The first and second stage operation cost of case 7 are \$759910 and \$248762, respectively. With the increase of *AIL*, the expected second stage costs increase rapidly. In particular, the expected second stage cost

TABLE II
PARAMETERS OF WATER RESERVOIRS

Node No.	$P_{wr,max}$ (m³/h)	λ_{wr} ($/m³)	Elevation (m)
1	325	6.4	-252.5
2	700	2.6	-255

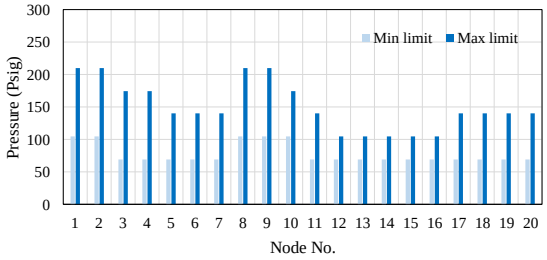

Fig. 3. Limits of gas pressure at each node.

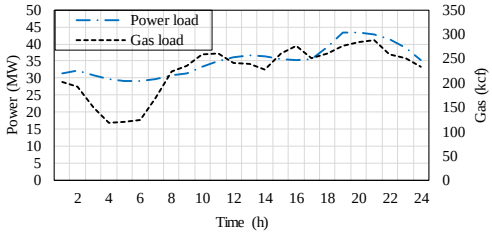

Fig. 4. Power and gas load profile.

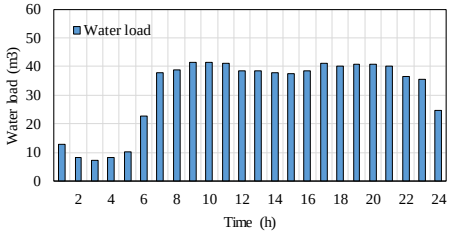

Fig. 5. Water load profile.

increases $637428 from case 9 to 10. Consequently, it can be concluded that the increase rate of operation cost is highly affected by the *AIL*.

B. Studies on Load Shedding

Load shedding in three sub-systems is implemented to ensure the overall system security and maintain the feasibility of the proposed mitigation scheme. The optimal coordinated load shedding strategy considers power load shedding (PLS), gas load shedding (GLS) and water load shedding (WLS) for 24 hours under different levels of FDIA. Figs. 6-9 present the load shedding under different combinations of FDIA. In Fig. 6, it can be seen that PLS is affected by both P-FDIA and G-FDIA. PLS is not sensitive when the *AIL* of P-FDIA is below 8%. When G-FDIA is at 0%, PLS rises from 0MWh to 691MWh; when G-FDIA is at 20%, PLS rises from 0MWh to 1274MWh. Fig. 7 shows the GLS under P-FDIA and G-FDIA. The highest GLS, 589kcf, is obtained when the two types of FDIA are at the highest level. When solely conducting G-FDIA, GLS ranges between 400kcf and 589kcf. The PLS under P-FDIA and W-FDIA is shown in Fig. 8. The highest PLS (1990MWh) is implemented at 20% of *AIL* of P-FDIA and W-FDIA, which

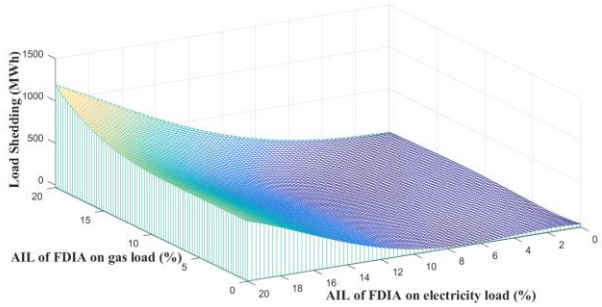

Fig. 6. Power load shedding under P-FDIA and G-FDIA.

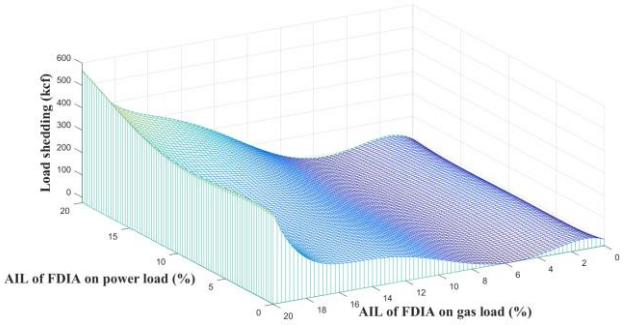

Fig. 7. Gas load shedding under P-FDIA and G-FDIA.

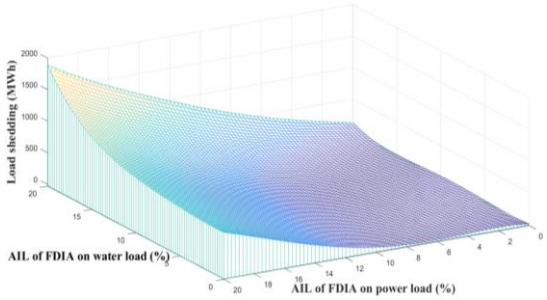

Fig. 8. Power load shedding under P-FDIA and W-FDIA.

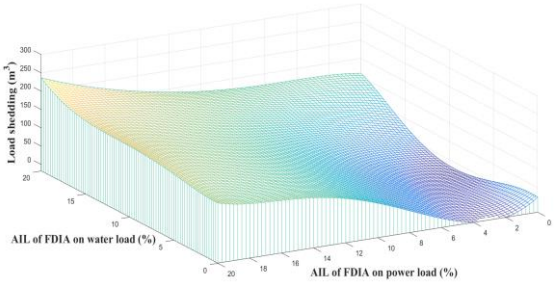

Fig. 9. Water load shedding under P-FDIA and W-FDIA.

indicates the higher impact caused by W-FDIA compared with G-FDIA in Fig. 6. At the highest level of P-FDIA, increasing W-FDIA causes PLS growth from 709MWh to 1990MWh. Fig. 9 depicts WLS under P-FDIA and W-FDIA. The highest WLS is 257m^3 at the highest level of P-FDIA and W-FDIA.

TABLE III
CASE ILLUSTRATION

Case No.	Optimization method	P-FDIA	G-FDIA	W-FDIA	Renewable Uncertainty	*AIL*
1	Deterministic	No	No	No	No	0%
2	RO	Yes	Yes	Yes	No	5%
3	RO	Yes	Yes	Yes	Yes	5%
4	DRO	Yes	No	No	No	5%
5	DRO	Yes	Yes	No	No	5%
6	DRO	Yes	Yes	Yes	No	5%
7	DRO	Yes	Yes	Yes	Yes	5%
8	DRO	Yes	Yes	Yes	Yes	10%
9	DRO	Yes	Yes	Yes	Yes	15%
10	DRO	Yes	Yes	Yes	Yes	20%

TABLE IV
ECONOMIC PERFORMANCE FOR CASE 1-10

Economic result	Case 1	Case 2	Case 3	Case 4	Case 5
First-stage cost ($)	843986	1031728	1037751	729817	748581
Expected Second-stage cost ($)	0	0	0	125279	133381
Total cost ($)	843986	1031728	1037751	855096	881962
Economic result	Case 6	Case 7	Case 8	Case 9	Case 10
First-stage cost ($)	759284	759910	804595	843697	889062
Expected Second-stage cost ($)	247276	248762	516593	994951	1632379
Total cost ($)	1006560	1008672	1321188	1838648	2521441

Compared with other FDIA scenarios, WLS increases smoothly when P-FDIA is at the highest level.

C. Scalability Analysis

In this section, the proposed TSRA-FMS is tested in a larger system scale to validate the applicability. This WES contains an IEEE 118-bus system, a 20-node gas system and a 10-node water system according to [32] and [33]. There are 54 power generators and 3 RES generators in the power system. RES generators are connected with buses 36, 69 and 77 with a capacity of 250MW. This analysis is conducted among 8 cases to demonstrate i) the effectiveness of TSRA-FMS on IESs, ii) comparison between risk-averse DRO and risk-neutral DRO and iii) the impact of system interdependency on system vulnerability. The case illustration is shown in TABLE V. Note that 'system interdependencies' indicates the number of connected gas and water systems in the WES. For instance, in case 1, the WES contains 3 gas systems and 3 water systems.

In Figs. 10 and 11, the water load shedding under cases 4 and 5 is given. Cases 4 and 5 are used to compare the proposed risk-averse DRO and risk-neutral DRO of [9]. In Fig. 11, the WLS reaches up to 983m^3 when P-FDIA and W-FDIA are both under 20% of *AIL*. When P-FDIA is not considered, the highest *AIL* of W-FDIA causes 77 m^3 WLS. Compared with Fig. 10, the risk-averse DRO presents a higher WLS than that of risk-neutral DRO, i.e., the WLS is 1168 m^3 under 20% of P-FDIA and W-FDIA, which is 19% higher than that of risk-neutral DRO.

TABLE V
CASE ILLUSTRATION

Case No.	Risk analysis	Test system	System interdependencies
1	Yes	IES	3
2	Yes	IES	2
3	Yes	IES	4
4	No	WES	3
5	Yes	WES	3
6	Yes	WES	2
7	Yes	WES	4

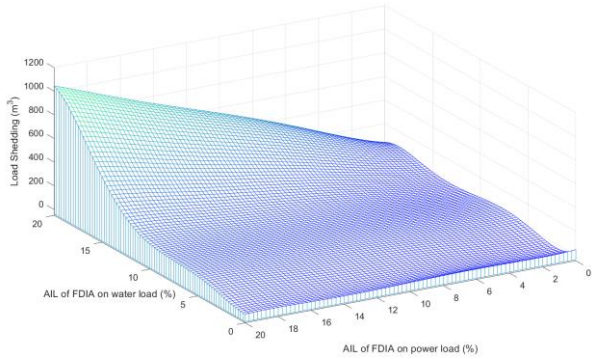

Fig. 10. Water load shedding under case 4.

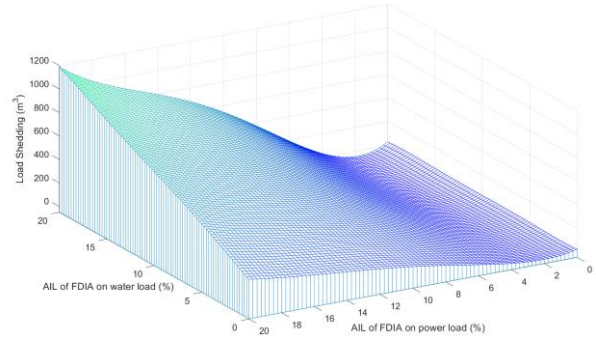

Fig. 11. Water load shedding under case 5.

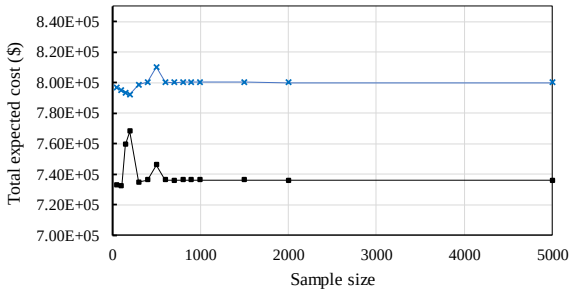

Fig. 12. Total expected cost of cases 4 and 5.

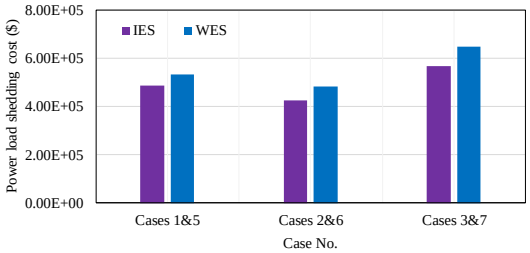

Fig. 13. Power load shedding cost of different cases.

5% of AIL is considered for Figs. 12 and 13. In Fig. 12, the second-stage expected cost under different sample size is given, where the black and blue curves represent cases 4 and 5, respectively. Overall, case 4 without considering CVaR shows lower second-stage expected operation cost under FDIA and renewable uncertainty. When 5000 second-stage samples are considered, the results of cases 4 and 5 approximates to $736000 and $800000. However, the result fluctuates when the data sample is below 500. In Fig. 13, the results show that the PLS in WES is higher than that in IES. For instance, cases 3 and 7 yield $567000 and $648000 PLS cost, respectively. Since W-FDIA causes WLS and the water reservoirs and pumps require higher usage. Accordingly, higher power consumption of water pumps leads to higher PLS. For case 5, there are 2 gas systems and 2 water systems, which shows $47000 higher cost than that of case 6 with 1 gas system and 1 water system. The additional 2 P2G facilities and 3 water pumps thus result in higher power consumption.

VI. Conclusion

Under the water-energy nexus era, the three proposed sub-systems are highly interwined. The cyber-attacks on any sub-system could propagate to the other two-subsystems. Consequently, this paper proposes a two-stage risk-based mitigation strategy for the novel WES under water-energy nexus. Both the day-ahead and real-time operation schemes are determined with FDIA on three sub-systems. The FDIA and renewable uncertainty are captured via the proposed RA-DRO. The trade-off between the economic performance and risk caused by cyber-attacks and renewable fluctuation is provided. This two-stage mitigation framework with flexible risk alternative is solved by a tractable Bender's decomposition method. Through the extensive studies, the key findings are listed below:

- Considering all types of FDIA, i.e., P-FDIA, G-FDIA and W-FDIA, leads to higher system economic loss than considering two types or one type of FDIA.
- PLS is more sensitive to W-FDIA compared with G-FDIA.
- The proposed RA-DRO mitigates the conservatism of RO with less load shedding.

The economic efficiency and system security under water-energy nexus is achieved via the effective proposed TSRA-FMS with optimally coordinated load shedding schemes to protect the entire system. The end energy users will benefit from this better supply security. This work is especially practical under smart cities with enormous water-energy interdependencies.

References

[1] A. Ashok, M. Govindarasu, and J. Wang, "Cyber-Physical Attack-Resilient Wide-Area Monitoring, Protection, and Control for the Power Grid," *Proceedings of the IEEE*, vol. 105, no. 7, pp. 1389-1407, 2017, doi: 10.1109/JPROC.2017.2686394.

[2] L. Che, X. Liu, and Z. Li, "Mitigating False Data Attacks Induced Overloads Using a Corrective Dispatch Scheme," *IEEE Transactions on Smart Grid*, vol. 10, no. 3, pp. 3081-3091, 2019, doi: 10.1109/TSG.2018.2817515.

[3] L. Che, X. Liu, Z. Li, and Y. Wen, "False Data Injection Attacks Induced Sequential Outages in Power Systems," *IEEE Transactions on Power Systems*, vol. 34, no. 2, pp. 1513-1523, 2019, doi: 10.1109/TPWRS.2018.2871345.

[4] J. Zhang, Z. Chu, L. Sankar, and O. Kosut, "Can Attackers With Limited Information Exploit Historical Data to Mount Successful False Data Injection Attacks on Power Systems?," *IEEE Transactions on Power Systems*, vol. 33, no. 5, pp. 4775-4786, 2018, doi: 10.1109/TPWRS.2018.2818746.

[5] J. Zhao, L. Mili, and M. Wang, "A Generalized False Data Injection Attacks Against Power System Nonlinear State Estimator and Countermeasures," *IEEE Transactions on Power Systems*, vol. 33, no. 5, pp. 4868-4877, 2018, doi: 10.1109/TPWRS.2018.2794468.

[6] A. S. Musleh, G. Chen, and Z. Y. Dong, "A Survey on the Detection Algorithms for False Data Injection Attacks in Smart Grids," *IEEE Transactions on Smart Grid*, pp. 1-1, 2019, doi: 10.1109/TSG.2019.2949998.

[7] X. Liu, L. Che, K. Gao, and Z. Li, "Power System Intra-Interval Operational Security under False Data Injection Attacks," *IEEE Transactions on Industrial Informatics*, pp. 1-1, 2019, doi: 10.1109/TII.2019.2954350.

[8] H. Shayan and T. Amraee, "Network Constrained Unit Commitment Under Cyber Attacks Driven Overloads," *IEEE Transactions on Smart Grid*, pp. 1-1, 2019, doi: 10.1109/TSG.2019.2904873.

[9] P. Zhao, C. Gu, and D. Huo, "Two-Stage Coordinated Risk Mitigation Strategy for Integrated Electricity and Gas Systems under Malicious False Data Injections," *IEEE Transactions on Power Systems*, pp. 1-1, 2020, doi: 10.1109/TPWRS.2020.2986455.

[10] Z. Yi, Y. Xu, J. Hu, M. Chow, and H. Sun, "Distributed, Neurodynamic-Based Approach for Economic Dispatch in an Integrated Energy System," *IEEE Transactions on Industrial Informatics*, vol. 16, no. 4, pp. 2245-2257, 2020, doi: 10.1109/TII.2019.2905156.

[11] Y. He, M. Shahidehpour, Z. Li, C. Guo, and B. Zhu, "Robust Constrained Operation of Integrated Electricity-Natural Gas System Considering Distributed Natural Gas Storage," *IEEE Transactions on Sustainable Energy*, vol. 9, no. 3, pp. 1061-1071, 2018, doi: 10.1109/TSTE.2017.2764004.

[12] P. Zhao, C. Gu, Z. Hu, X. I. E. D, I. Hernando-Gil, and Y. Shen, "Distributionally Robust Hydrogen Optimization with Ensured Security and Multi-Energy Couplings," *IEEE Transactions on Power Systems*, pp. 1-1, 2020, doi: 10.1109/TPWRS.2020.3005991.

[13] P. Zhao *et al.*, "Volt-VAR-Pressure Optimization of Integrated Energy Systems with Hydrogen Injection," *IEEE Transactions on Power Systems*, pp. 1-1, 2020, doi: 10.1109/TPWRS.2020.3028530.

[14] M. Shahidehpour, Y. Zhou, Z. Wei, S. Chen, Z. Li, and G. Sun, "Distributionally Robust Co-optimization of Energy and Reserve for Combined Distribution Networks of Power and District Heating," *IEEE Transactions on Power Systems*, pp. 1-1, 2019, doi: 10.1109/TPWRS.2019.2954710.

[15] P. Zhao, C. Gu, D. Huo, Y. Shen, and I. Hernando-Gil, "Two-Stage Distributionally Robust Optimization for Energy Hub Systems," *IEEE Transactions on Industrial Informatics*, vol. 16, no. 5, pp. 3460-3469, 2020, doi: 10.1109/TII.2019.2938444.

[16] M. Asensio and J. Contreras, "Stochastic Unit Commitment in Isolated Systems With Renewable Penetration Under CVaR Assessment," *IEEE Transactions on Smart Grid*, vol. 7, no. 3, pp. 1356-1367, 2016, doi: 10.1109/TSG.2015.2469134.

[17] L. Yang, J. Jian, Y. Xu, Z. Dong, and G. Ma, "Multiple Perspective-Cuts Outer Approximation Method for Risk-Averse Operational Planning of Regional Energy Service Providers," *IEEE Transactions on Industrial Informatics*, vol. 13, no. 5, pp. 2606-2619, 2017, doi: 10.1109/TII.2017.2710055.

[18] S. Shin *et al.*, "A systematic review of quantitative resilience measures for water infrastructure systems," *Water*, vol. 10, no. 2, p. 164, 2018.

[19] V. M. Leiby and M. E. Burke, *Energy efficiency best practices for North American drinking water utilities*. WRF, 2011.

[20] A. S. Zamzam, E. Dall'Anese, C. Zhao, J. A. Taylor, and N. D. Sidiropoulos, "Optimal Water–Power Flow-Problem: Formulation and Distributed Optimal Solution," *IEEE Transactions on Control of Network Systems*, vol. 6, no. 1, pp. 37-47, 2019, doi: 10.1109/TCNS.2018.2792699.

[21] Q. Li, S. Yu, A. S. Al-Sumaiti, and K. Turitsyn, "Micro Water–Energy Nexus: Optimal Demand-Side Management and Quasi-Convex Hull Relaxation," *IEEE Transactions on Control of Network Systems*, vol. 6, no. 4, pp. 1313-1322, 2019, doi: 10.1109/TCNS.2018.2889001.

[22] C. Wang, N. Gao, J. Wang, N. Jia, T. Bi, and K. Martin, "Robust Operation of a Water-Energy Nexus: A Multi-energy Perspective," *IEEE Transactions on Sustainable Energy*, pp. 1-1, 2020, doi: 10.1109/TSTE.2020.2971259.

[23] Y. Yuan, Z. Li, and K. Ren, "Quantitative Analysis of Load Redistribution Attacks in Power Systems," *IEEE Transactions on Parallel and Distributed Systems*, vol. 23, no. 9, pp. 1731-1738, 2012, doi: 10.1109/TPDS.2012.58.

[24] C. Toro and E. Sciubba, "Sabatier based power-to-gas system: Heat exchange network design and thermoeconomic analysis," *Applied Energy*, vol. 229, pp. 1181-1190, 2018/11/01/ 2018, doi: https://doi.org/10.1016/j.apenergy.2018.08.036.

[25] T. Haktanır and M. Ardıçlıoğlu, "Numerical modeling of Darcy–Weisbach friction factor and branching pipes problem," *Advances in Engineering Software*, vol. 35, no. 12, pp. 773-779, 2004.
[26] R. T. Rockafellar and S. Uryasev, "Optimization of conditional value-at-risk," *Journal of risk*, vol. 2, pp. 21-42, 2000.
[27] R. A. Jabr, "Robust self-scheduling under price uncertainty using conditional value-at-risk," *IEEE Transactions on Power Systems*, vol. 20, no. 4, pp. 1852-1858, 2005, doi: 10.1109/TPWRS.2005.856952.
[28] S. Uryasev and R. T. Rockafellar, "Conditional value-at-risk: optimization approach," in *Stochastic optimization: algorithms and applications*: Springer, 2001, pp. 411-435.
[29] S. Zhu and M. Fukushima, "Worst-case conditional value-at-risk with application to robust portfolio management," *Operations research*, vol. 57, no. 5, pp. 1155-1168, 2009.
[30] S. Dempe, "Directional differentiability of optimal solutions under Slater's condition," *Mathematical Programming*, vol. 59, no. 1-3, pp. 49-69, 1993.
[31] A. Ruszczyński and A. Shapiro, "Optimality and duality in stochastic programming," *Handbooks in Operations Research and Management Science*, vol. 10, pp. 65-139, 2003.
[32] I. I. o. T. Electrical and Computer Engineering Department. "Index of /data." motor.ece.iit.edu/data/ (accessed.
[33] D. COHEN, U. SHAMIR, and G. SINAI, "Optimal operation of multi-quality water supply systems-II: The QH model," *Engineering Optimization+ A35*, vol. 32, no. 6, pp. 687-719, 2000.